

RESEARCH ARTICLE

An optical flow battery enabled by trap-engineered nanophosphors

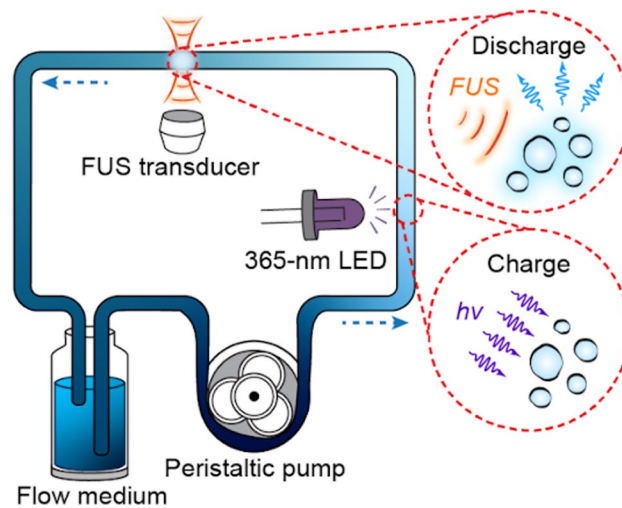
Xiang Wu^{1,2} · Fan Yang^{1,2} · Zihao Ou^{1,2} · Guosong Hong^{1,2}

Received: 2 August 2024 / Revised: 15 September 2024 / Accepted: 20 September 2024 / Published online: 2 December 2024
© The Author(s) 2024

Abstract

Flow batteries represent a promising technology for storing electrical energy in circulating electrolyte solutions that contain redox-active chemicals. Inspired by the redox flow battery, in this paper we describe the concept and implementation of an optical flow battery, which stores photon energy in circulating nanophosphor colloids. Similar to the redox flow battery, the optical flow battery enables the conversion between photon energy and chemical energy in a rechargeable manner, facilitating distributed energy storage by decoupling energy and power. We characterized basic cell attributes and performance metrics of this prototype optical flow battery in the context of common assessment methods for conventional redox flow batteries. We envision that this optical flow battery may provide a useful tool for solar energy storage, light delivery in live animals, and light-based therapy, diagnosis, and surgery in medicine.

Graphical Abstract



Highlights

- An optical flow battery can enable in vivo light delivery for light-based therapy, diagnosis, and surgery in medicine.

Xiang Wu and Fan Yang contributed equally to this work.

✉ Guosong Hong
guosongh@stanford.edu

¹ Department of Materials Science and Engineering, Stanford University, Stanford, CA 94305, USA

² Wu Tsai Neurosciences Institute, Stanford University, Stanford, CA 94305, USA



Keywords Mechanoluminescence · Biophotonics · Light delivery

Introduction

Flow batteries are important energy storage systems that store electrical energy in redox-active chemicals dissolved in circulating media [1]. Redox flow batteries benefit from their large capacity proportional to tank size and stable power output resulting from continuous circulation of electrolyte solutions. Owing to these advantages, flow batteries represent a promising technology for large-scale energy storage. When a redox flow battery is charged and discharged, electrical energy is converted to and from chemical energy, respectively, in a rechargeable manner [2].

We hypothesize that an analog of the redox flow battery operating in the optical domain exists to reversibly convert photon energy to and from chemical energy stored in a circulating medium. There are two main drives for the development of an optical flow battery. First, although solar flow batteries enable light harvesting via the monolithic integration of photovoltaics with redox flow batteries [3], an additional light-to-electricity conversion is involved during charging while photons are no longer recovered during discharging. The simplest optical flow battery should involve direct conversion between photon energy and chemical energy to enable both light input and output. Second, we envision that a miniature optical flow battery may enable numerous applications as a medical implant, since *in vivo* light delivery to deep tissues represents a main challenge for photodynamic therapy [4], light endoscopy [5], optogenetics [6], and light-activated gene editing [7]. Therefore, developing an all-optical flow battery expands the arsenal of energy storage devices and light delivery systems available to energy scientists and biomedical researchers.

In this work, we demonstrate the first prototype of an optical flow battery in an artificial circulatory system. This artificial circulatory system contains a circulating medium made of trap-engineered nanophosphors with small particle sizes to facilitate their continuous flow and engineered point defects to store and release photon energy reversibly. We characterized basic cell attributes and performance metrics of this prototype optical flow battery following previous reports of conventional redox flow batteries. We envision that this optical flow battery may provide a useful tool for solar energy storage, *in vivo* light delivery, and light-based therapy, diagnosis, and surgery in medicine.

Results and discussion

The design of the optical flow battery (Fig. 1a) comprises photoexcitation, a flow medium that stores optical energy, and emission gated by an external stimulus such as focused

ultrasound (FUS). As a result, an optical flow battery can be considered as a time-delayed photoluminescent system where photoexcitation and FUS-stimulated emission are two separate and independent processes. In this sense, the optical flow battery is akin to a redox flow battery, the latter of which stores electrical energy in redox species with separate and independent recharging and discharging processes.

Central to the optical flow battery is the flow medium that stores optical energy and must meet two requirements. First, the flow medium must be a liquid with stable suspension of its content and low viscosity to facilitate continuous flow and transport of the energy-storing material. Second, the flow medium must be optically active to store photoexcitation energy via certain photophysical and/or photochemical mechanisms and release this energy under external stimuli. We have identified one of such flow media that comprises a colloidal solution of strontium magnesium silicate nanoparticles doped with europium(II) and dysprosium(III) ($\text{Sr}_2\text{MgSi}_2\text{O}_7\text{:Eu,Dy}$, SMSO). SMSO is a solid-state material that has been reported to exhibit mechanoluminescence in its bulk form [8]. Specifically, point defects arising from dopant ions in SMSO act as electron and hole traps to store photoexcitation energy, which can be released as light emission under external mechanical stress, such as under incident FUS (Fig. 1b). As a result, SMSO satisfies the second requirement of optical energy storage. However, the large sizes ($> 10 \mu\text{m}$) of the bulk SMSO material synthesized from solid-state reactions prevent their use in a flow medium since they cannot be stably suspended in a liquid, thus disqualifying this bulk material for the first requirement.

To address this challenge, our lab has recently developed a biomineral-inspired suppressed dissolution approach for producing nanophosphors down to 20 nm from their bulk counterparts [9–11]. These nanophosphors retain the desired photophysical properties such as persistent luminescence and mechanoluminescence from their bulk precursors, while their small size distribution yields stable colloidal solutions in water. Therefore, SMSO nanophosphor colloids act as a potential flow medium to realize an optical flow battery by satisfying both requirements above. To validate their capability in an optical flow battery, we characterized the size distribution and crystallographic structure of SMSO nanophosphors with transmission electron microscopy (TEM) and high-resolution transmission electron microscopy (HRTEM), respectively (Fig. 1c). An average size of $49 \pm 18 \text{ nm}$ was found for SMSO nanophosphors produced by the biomineral-inspired suppressed dissolution approach (Fig. 1d),

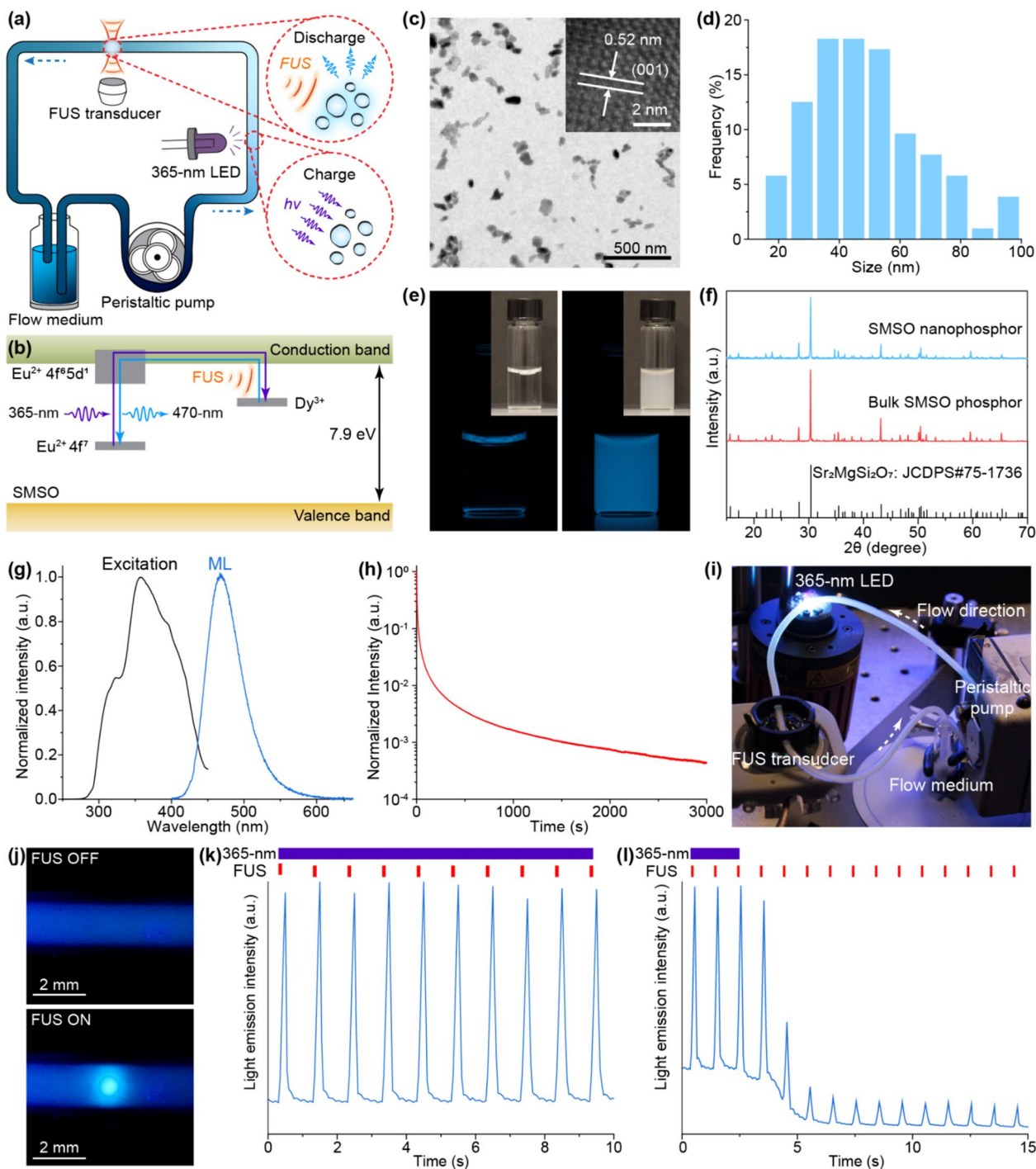


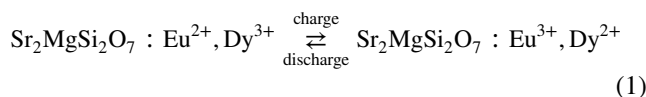
Fig. 1 Design and implementation of the optical flow battery. **a** Schematic showing the design of the optical flow battery. **b** Schematic illustrating the mechanism of Dy^{3+} -assisted trapping of photoexcitation energy and FUS-mediated detrapping, yielding light emission in the SMSO material. **c** TEM image of SMSO nanophosphor colloids. The inset shows an HRTEM image of SMSO nanophosphor colloids. **d** The size distribution of SMSO nanoparticles in **(c)**. **e** Luminescence and brightfield (insets) images of the bulk SMSO phosphor (left) and nanophosphor colloids (right) suspended in water. Note that due to the large sizes of the bulk SMSO phosphor, a stable suspension could not be achieved, yielding precipitation of the bulk SMSO phosphor. **f** XRD spectra of the bulk SMSO phosphor and nanophosphor. **g** Excitation and mechanoluminescence (ML) spectra of the SMSO nanophosphor. **h** Afterglow decay curve of the SMSO nanophosphor. **i** A photo showing the setup of an optical flow battery. **j** Luminescence images showing strong mechanoluminescence emission at the ultrasound focus (bottom), in contrast to the weak persistent luminescence background in the absence of ultrasound (top). **k, l** Time-resolved light intensity measurements with **(k)** or without **(l)** continuous 365-nm recharging light. The baseline drop in **l** after the UV light is turned off comes from the gradual decay of SMSO nanophosphors afterglow. The purple bar represents 365-nm recharging light, while red ticks indicate discharging FUS pulses

thus supporting their superior colloidal stability over bulk SMSO phosphors (Fig. 1e). The crystallographic structure of SMSO nanophosphors was confirmed in the X-ray diffraction (XRD) pattern, which exhibits identical peaks to the bulk material (Fig. 1f).

We next sought to characterize the optical properties of SMSO colloids to satisfy the second requirement for an optical flow battery. Specifically, the strong absorption of SMSO colloids near 365 nm (Fig. 1g, left) and their long luminescence lifetime (Fig. 1h) suggest their ability to store the photoexcitation energy provided by ultraviolet (UV) light. In addition, the mechanoluminescence spectrum of SMSO colloids under FUS exhibited a peak at 470 nm, thus confirming their ability to release the stored optical energy with ultrasound stimuli (Fig. 1g, right).

Having demonstrated that SMSO colloids satisfy both requirements, we sought to implement an optical flow battery using these colloids. This optical flow battery comprises a Tygon tubing filled with SMSO colloids at a concentration of 25 mg/mL, a peristaltic pump that drives the flow, a 365-nm light emitting diode (LED) that provides photoexcitation, and an ultrasound transducer with its focus inside the tubing (Fig. 1i). Flowing colloids produce intense blue emission, which corresponds to the mechanoluminescence spectrum of SMSO, upon FUS stimulation (Fig. 1j). We validated the necessity of continuous photoexcitation to produce reproducible light output by measuring the time trace of light intensity at the ultrasound focus (Fig. 1k & l). Importantly, the stable intensity of FUS-triggered light emission under continuous recharging suggests that a steady state is established between the energy input vs output, thus fulfilling the role of an optical flow battery. The photochemical reactions during charging and discharging of this optical flow battery are shown in

Eq. (1), with a ΔG of -1.528 kJ/mol $\text{Sr}_2\text{MgSi}_2\text{O}_7:\text{Eu,Dy}$ for the discharging process.



We measured basic attributes and performance metrics of the optical flow battery by benchmarking it against standard redox flow batteries. Specifically, we evaluated the state of charge (SOC) and output emission power as two fundamental attributes of the optical flow battery pertinent to its energy storage capability and output efficiency, respectively. First, SOC is defined as charged capacity stored over theoretical capacity in redox flow batteries [1], and in the optical flow battery, SOC represents the percentage of occupied traps over all traps predicted by the stoichiometry of doping in SMSO [12]. We measured the total number of emitted photons by integrating the emission of SMSO colloids after recharging them with 365-nm photoexcitation of varied power density and duration. Dividing this integrated photon number by the total number of Eu^{2+} ions, which are believed to be the origin of trapped charges in similar phosphor materials,¹³ yields the SOC value in our measurements. Figure 2a reveals that SOC is a function of both the power density and duration of photoexcitation, with a maximum SOC of 6.5% achieved after 1 mW/mm² photoexcitation for 30 s. Importantly, this maximum SOC agrees with the absolute storage capacity, 1.6%, of a similar material, $\text{SrAl}_2\text{O}_4:\text{Eu,Dy}$ [13]. Compared to redox flow batteries, the limited SOC of our optical flow battery is a result of several competing processes. Specifically, non-radiative processes of trap relaxation [13], as well as the “leaky bag” model of afterglow luminescence [14], may have contributed to this limited SOC.

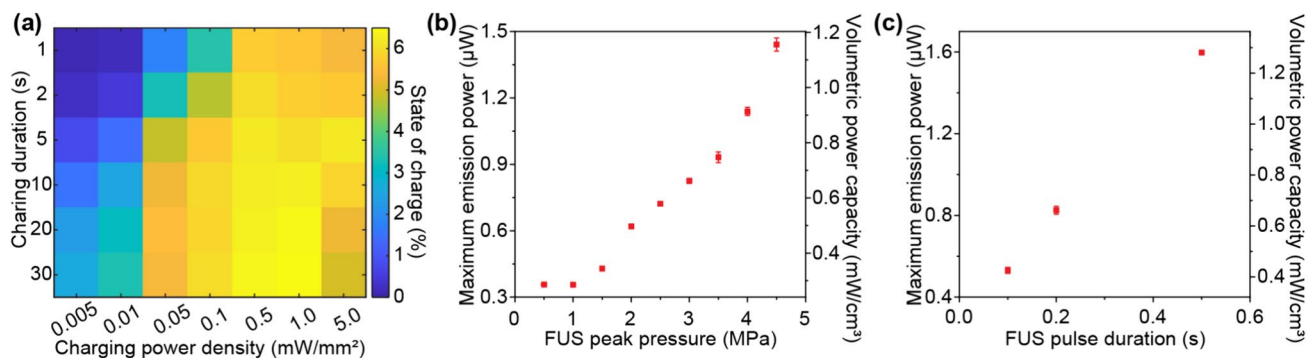


Fig. 2 State of charge and maximum emission power of the optical flow battery. **a** A heatmap showing the state of charge of SMSO nanoparticles at different charging durations and power densities. The state of charge decreases when the charging power density increases from 1 mW/mm² to 5 mW/mm² because the heating effect of the UV recharging light becomes significant at 5 mW/mm². **b, c** The maximum emission power and volumetric power capacity of the optical flow battery with different FUS peak pressures (**b**) and pulse durations (**c**). The FUS pulse duration was 200-ms for (**b**) and the FUS peak pressure was 3-MPa for (**c**). The data are represented as mean \pm standard deviation (SD) from 10 independent measurements

Besides the SOC, we also measured the maximum emission power from the optical flow battery as a function of the peak pressure and duration of applied ultrasound pulses (Fig. 2b & c, left y axis). We found an increasing trend of the maximum emission power with intensifying and prolonged FUS pulses, with the highest emission power of $1.6 \mu\text{W}$ from the ultrasound focus achieved at 3-MPa pressure and 500-ms duration of ultrasound. The resulting power density contributed by a single tubing on its surface was calculated to be $2.0 \mu\text{W}/\text{mm}^2$, sufficient for activating many light-sensitive proteins such as photoactivatable Cas9 [7]. Since the emission power reflects the discharge capacity in the flow medium, we also quantified the volumetric power capacity of our optical flow battery by dividing the emission power by the volume of ultrasound focus in the flowing medium (Fig. 2b & c, right y axis). A maximum volumetric power capacity of $1.3 \text{ mW}/\text{cm}^3$ was found.

Further characterizations of the basic attributes of the optical flow battery in Fig. 2 allows us to evaluate its performance. The first metric we used to evaluate its performance is the energy extraction efficiency, which is equivalent to the Coulombic efficiency and energy efficiency of a redox flow battery. We used a single efficiency to characterize the optical flow battery since the cell voltage, which is an important parameter in the redox flow battery, does not apply to the optical flow battery. We plotted the energy extraction efficiency, which is defined as the ratio of the discharge capacity over the charge capacity, as a function of time within each discharging cycle with the peak pressure and duration of FUS stimuli as two independent parameters (Fig. 3a & b). In general, the energy extraction efficiency increases and approaches 13.6% as the FUS stimulus intensifies and extends. We attributed this low energy extraction efficiency to the spontaneous emission, also known as persistent luminescence, of SMSO colloids (Fig. 1h). This

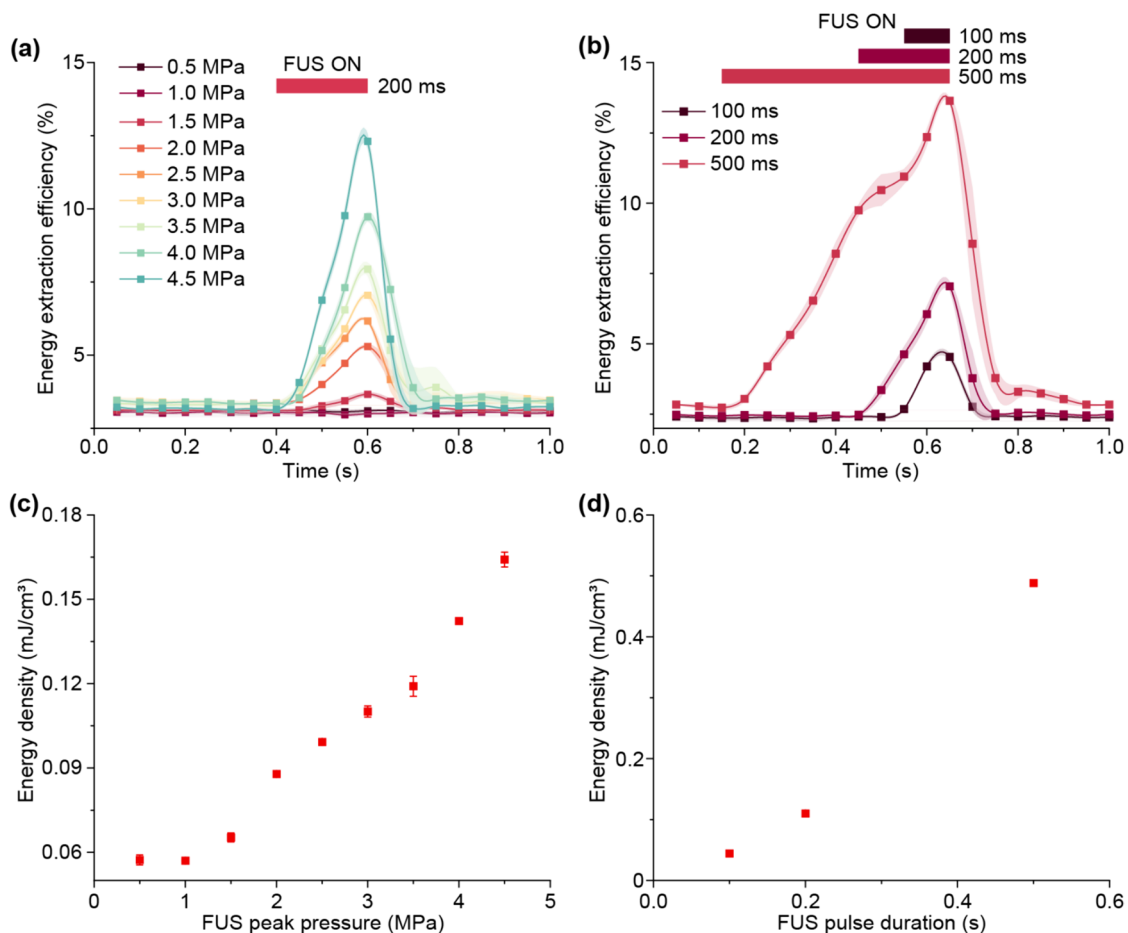


Fig. 3 Energy extraction efficiency and energy density of the optical flow battery. **a, b** The energy extraction efficiency of the optical flow battery averaged over multiple discharging cycles with different FUS peak pressures (**a**) and pulse durations (**b**). The shadow represents the standard deviation (SD) from 10 individual measurements. The red bars on the top indicate the duration of FUS pulses. **c, d** The energy density of the optical flow battery with different FUS peak pressures (**c**) and pulse durations (**d**). The data are represented as mean \pm SD from 10 independent measurements. The FUS pulse duration was 200-ms for (**a, c**) and the FUS peak pressure was 3-MPa for (**b, d**)

unfavorable spontaneous emission process is a main contributor to efficiency loss of the optical flow battery, akin to the self discharge process in redox flow batteries. We then used the energy density as the second metric of our system and studied how it varies with the peak pressure and duration of FUS stimuli. Similar to redox flow batteries, energy density is defined as energy output per unit volume of the flow medium, integrated over the entire duration of a discharging pulse. Figure 3c & d reveal an energy density in the range of 44–488 $\mu\text{J}/\text{cm}^3$ per discharging pulse of the optical flow battery.

Besides the energy extraction efficiency and energy density, another important metric for characterizing the performance of a flow battery is the capacity decay rate, which reflects the lifetime of the device. To this end, we measured light emission intensity at the ultrasound focus over repeated discharging cycles when the recharging photoexcitation is constantly on (Fig. 4 a,b). After a steady state was established between energy input and output, a consistent output intensity of the optical flow battery was found over at least 3600 cycles or 60 min (Fig. 4c). However, a slow decay in the output light intensity was observed over 8 h, yielding a power decay rate of 0.001% per cycle or 0.06% per min

(Fig. 4c, left y axis). This decay in output light intensity results in a gradual decrease in volumetric power capacity (Fig. 4c, right y axis) and energy extraction efficiency per discharge cycle (Fig. 4d). We attributed this time-dependent decay to the gradual evaporation of the water-based ultrasound gel and the cumulative displacement of the tubing due to the acoustic radiation pressure, which can be further optimized by constantly supplying fresh ultrasound gel and fixing the tubing position.

We summarized the key attributes and performance metrics of our optical flow battery in Table 1. In comparison, commercial redox flow batteries can operate at an SOC up to 100% and an energy extraction efficiency > 90%. As a result, the performance characteristics of the optical flow battery reported in this work warrant further improvement for practical energy storage applications. Despite its suboptimal performance, our optical flow battery in this work represents the first prototype of this device by demonstrating the feasibility of converting photon energy with chemical energy in a reversible manner. Therefore, this prototype offers an alternative to conventional redox flow batteries by operating in the optical domain, expanding the arsenal of energy storage devices and light delivery systems available to energy

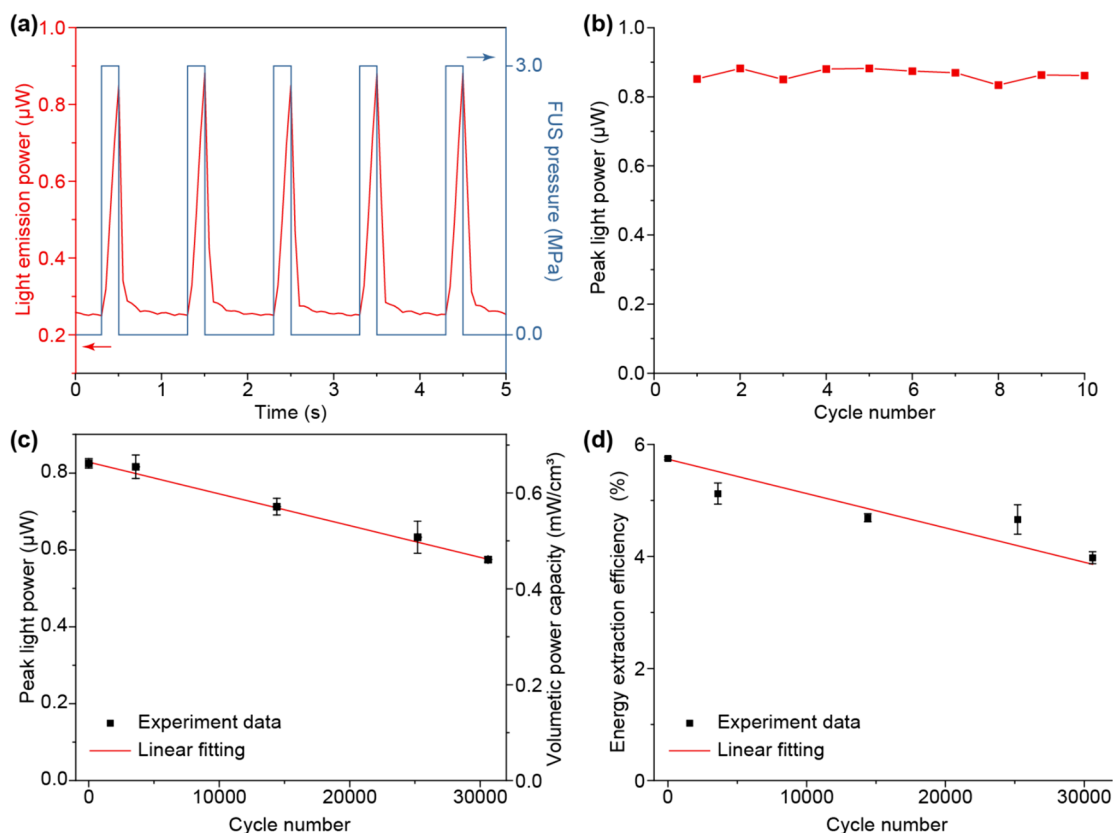


Fig. 4 The lifetime and stability of the optical flow battery. **a** Time-resolved light emission power and FUS pressure of the optical flow battery. **b** Peak emission power for the first 10 charge/discharge cycles. **c**, **d** Peak emission power, volumetric power capacity (**c**), and energy extraction efficiency (**d**) for over 30,000 cycles. The data are represented as mean \pm standard deviation (SD) from 5 independent measurements

Table 1 Cell attributes and performance metrics of optical flow battery

Cell attributes	
Theoretical capacity	4.2 J/g
SOC	6.5%
Performance metrics	
Volumetric power capacity	1.3 mW/cm ³
Capacity decay rate	0.001% per cycle; 0.06% per min
Energy extraction efficiency	13.6%
Energy density	488 μJ/cm ³

scientists and biomedical researchers. Future improvements of the optical flow battery should leverage nanophosphors engineered with deeper traps and suppressed nonradiative relaxation of traps, thus mitigating competing processes leading to self-discharge of the system. Specifically, creating deeper traps in nanophosphor colloids helps reduce spontaneous photoluminescence and persistent luminescence during and after recharging, respectively, thus improving the SOC and energy extraction efficiency of the system. In addition, suppressing nonradiative relaxation of traps improves the quantum efficiency of mechanoluminescence, yielding a higher emission power, volumetric power capacity, and energy density during FUS-stimulated discharge.

This prototype optical flow battery is highly suitable for large-scale production. Specifically, we used the suppressed dissolution approach to produce the SMSO nanophosphors from the bulk SMSO precursors, which can be produced in large quantities using solid state reactions [9, 10]. Furthermore, the suppressed dissolution approach only involves a one-step wet-chemical reaction, is straightforward to implement, and only requires low-cost chemicals such as citric acid. Additionally, the suppressed dissolution approach is widely utilized by biological organisms to produce nanostructures, and thus have very low environmental impact. Apart from material production, to integrate the optical flow battery into larger systems simply requires larger circulating tubing and more powerful ultrasound transducers, both of which are common and commercially available. Therefore, we envision that the optical flow battery has great potential for low-cost scaling up and commercialization.

Although the current performance metrics of the optical flow battery prohibit its use for large-scale energy storage, its many features enable unique applications in biology and medicine. Specifically, the ability to store photon energy in this flow device makes it possible to deliver light of desired wavelengths to the body for manipulating and monitoring many biological processes via optogenetics [6, 15], photodynamic therapy [4], light-activated gene editing [7, 16], and light endoscopy [5]. The similarity between a

flow battery and the endogenous circulatory system in the mammalian body implies the potential to design a bioinspired optical flow battery. Inside the body, the continuous pumping of oxygen-rich blood to energy-consuming organs enables oxidative metabolism to occur at a constant rate under homeostasis, thus fulfilling the role of the endogenous circulatory system as a redox flow battery. Inspired by this structural and functional similarity, we hypothesize that the endogenous circulatory system in the mammalian body can be turned into an optical flow battery. Specifically, blood vessels may be leveraged to replace the Tygon tubing in Fig. 1i, where blood acts as an intrinsic flow medium to carry trap-engineered phosphor colloids [17]. After systemic delivery of SMSO, superficial blood vessels near the skin act as a solar panel to absorb photoexcitation light and SMSO colloids flowing in the blood act as the medium to store the absorbed photon energy. Finally, tissue-penetrant FUS discharges the battery to emit light at any depth or location inside the body with spatiotemporal precision, thus fulfilling the purpose of internal light delivery in living organisms. However, we also note that a few important factors need to be considered when applying this optical flow battery in vivo: First, surface functionalization of the SMSO nanophosphors (e.g. with polyethylene glycol) would be needed to improve their circulation lifetime in the bloodstream. Second, the pharmacokinetics of the SMSO nanophosphors need to be carefully studied to ensure negligible toxicity. Third, since the SMSO nanophosphors will be circulating in the blood vessels, the light emission intensity triggered by FUS pulses in vivo will depend on the volume percentage of blood, which is highly inhomogeneous across different organs. Lastly, the scalability of the SMSO nanophosphors needs to be further optimized for potential clinical applications, since a single dose of intravenous injection in humans would require 1–2 orders of magnitude more SMSO nanophosphors than the amount used in the current optical flow battery prototype.

Conclusion

The first working prototype of an optical flow battery has been demonstrated in this work. This optical flow battery uses trap-engineered nanophosphor colloids suspended in an aqueous flow medium as the energy storage material, which absorb photon energy during the charging phase and emit light during the discharging phase. In steady-state operation, the optical flow battery can be charged to a maximum SOC of 6.5% and discharged by FUS to a maximum power of 1.6 μW. Under optimized discharging conditions, the optical flow battery exhibits a volumetric power capacity of 1.3 mW/cm³, an energy extraction efficiency of 13.6%, and an energy density of 488 μJ/cm³. With a capacity decay rate of

0.001% per cycle, this device operates with stable output light intensity over at least 60 min. We anticipate further improvements of the optical flow battery by suppressing competing self-discharge processes such as spontaneous emission and nonradiative decay. We envision that an *in vivo* optical flow battery can be realized by systemically delivering an optical storage medium in the intrinsic circulatory system. This endogenous optical flow battery may enable spatiotemporally precise light delivery to deep tissues of the body, thus facilitating *in vivo* optogenetics, photodynamics therapy, and light-activated gene editing with minimal invasiveness and light relocation ability.

Experimental section

Synthesis of $\text{Sr}_2\text{MgSi}_2\text{O}_7\text{:Eu,Dy}$ (SMSO) colloids in water

SMSO colloids were synthesized from bulk SMSO phosphors via a previously reported biomineral-inspired suppressed dissolution approach [9–11]. Briefly, SMSO bulk phosphors were prepared via a solid-state reaction. Specifically, 7.9 mmol of SrCO_3 , 0.8 mmol of $(\text{MgCO}_3)_4\cdot\text{Mg}(\text{OH})_2\cdot 5\text{H}_2\text{O}$, 8 mmol of SiO_2 , 0.012 mmol of Eu_2O_3 , 0.04 mmol of Dy_2O_3 , and 0.24 mmol of H_3BO_3 were thoroughly ground and then annealed at 1100 °C for 2 h under 5% H_2/Ar . The as-obtained SMSO bulk phosphors were ground in a high energy ball mill for 30 min. After that, 200 mg of ballmilled SMSO particles were added into 24 mL of the suppressed-dissolution solution (sodium citrate buffer, 0.08 mol/L, pH=6) and stirred at 80 °C for 72 h. The final SMSO nanophosphor colloids were separated from bulk precursors by centrifugation at 1000 rpm for 10 min.

Structural and compositional characterizations of SMSO colloids

These characterizations include TEM, HRTEM, and XRD. TEM and HRTEM images of SMSO colloids were acquired by a Field Electron and Ion Company Tecnai TEM microscope. The XRD pattern of SMSO colloids was collected by a X-ray PANalytical Empyrean diffractometer. The concentration of SMSO colloids was determined by a X-SERIES II Quadrupole inductively coupled plasma mass spectrometer (ICP-MS).

Optical characterizations of SMSO colloids

These characterizations include photoexcitation spectrum, mechanoluminescence spectrum, and afterglow decay curve. The excitation spectrum of SMSO colloids was measured by a Horiba FluoroLog spectrophotometer. The mechanoluminescence spectrum of SMSO nanophosphors was measured by doping them in a polydimethylsiloxane (PDMS)

phantom. Specifically, a PDMS phantom with a thickness of 0.2 mm was uniformly doped with 70 mg/mL SMSO nanoparticles and used for mechanoluminescence spectrum and afterglow decay curve measurements. For the mechanoluminescence spectrum, the PDMS phantom was placed at the focus of an ultrasound transducer (Image Guided Therapy, Pessac, France) and charged for 10 s by a 365-nm LED at 0.5 mW/mm². The central frequency of the transducer was 1.5 MHz. FUS pulses with a 1-Hz repetition rate were applied immediately after charging light was turned off, and the mechanoluminescence spectrum was acquired using a fiber-coupled spectrometer (OCEAN-HDX-VIS-NIR; Ocean Optics, Orlando, FL). Averaging over 5 measurements was applied to reduce the noise of the spectrum. For the afterglow decay curve measurement, the PDMS phantom was charged with a 365-nm LED for 10 s at 0.13 mW/mm², followed by time-resolved light collection by a photomultiplier tube (PMT1001; Thorlabs, Newton, NJ) immediately after charging was terminated. The output voltage from the PMT was then collected as a function of time using a multifunction input/output (I/O) device (NI USB-6221, National Instruments, Austin, TX).

Construction of the optical flow battery

Tygon tubing (inner diameter = 1.59 mm, outer diameter = 3.18 mm; Ryan Herco Flow Solutions, Burbank, CA) was used as the main body of the optical flow battery as shown in Fig. 1a & i. To completely eliminate any air bubbles inside the tube, we immerse the two ends of the tubing into a 2-mL glass vial filled with a 25 mg/mL solution of SMSO nanophosphors. A peristaltic pump (Model 720; Harvard Apparatus, Holliston, MA) was used to provide the driving force for the solution to circulate with a flow rate of 3.85 mL/min. To ensure that the same part of the tubing always stays at the focus of ultrasound, we designed a 3D-printed tube holder to fix the tubing position. A 365-nm LED (M365LP1; Thorlabs, Newton, NJ) was used as the recharging light.

State of charge (SOC) measurements under different charging conditions

The PDMS phantom as prepared above was charged with a 365-nm LED (SOLIS-365C, Thorlabs, Newton, NJ) at different power densities and durations. At 1 s after the charging, an electron-multiplying CCD (EMCCD), iXon Ultra 888, Andor Technology, Belfast, United Kingdom) was exposed for 50 ms to capture an afterglow image of the phantom by setting the readout mode to be “photon counts”. The total number of photons from the phantom was integrated, corrected for the solid angle of the imaging system, and converted into energy. Using the afterglow decay curve

of SMSO (Fig. 1h), the energy storage capacity per gram of SMSO colloids at different charging conditions was then estimated. The theoretical capacity of SMSO was estimated to be 4.2 J/g by assuming all Eu^{2+} dopants donate one electron each to Dy^{3+} traps. The SOC was then calculated by taking the ratio of the experimentally measured energy storage capacity of SMSO and the theoretical capacity.

Maximum emission power and volumetric power capacity measurements under different discharging conditions

FUS pulses (1-Hz repetition rate) with different pressures and durations were applied to the tubing of the optical flow battery, and the mechanoluminescence from the ultrasound focus was acquired using the EMCCD with a 45.5-ms exposure time and 20-Hz frame rate in the “photon counts” read-out mode. The total number of photons was integrated over the FUS focal area, corrected for the solid angle and attenuation, and converted into energy. The emission power was then calculated by dividing the energy with the exposure time of a single frame. The volumetric power capacity was calculated by dividing the emission power by the volume of the FUS focus.

Determination of energy extraction efficiency

The energy extraction efficiency was calculated by dividing the emitted photon energy per image frame with the total energy stored in the SMSO fluid within the volume of the FUS focus. The total energy stored in the SMSO fluid was estimated using the corresponding charging condition and the SOC results (Fig. 2a).

Determination of energy density

The total emitted light energy from the optical flow battery per FUS pulse was calculated by integrating the emitted light energy over the on-phase of the FUS pulse. It was then divided by the focal volume of FUS to obtain the energy density.

Cycling measurements of the optical flow battery

FUS pulses with 200-ms duration, 3-MPa pressure and 1-Hz repetition rate were continuously applied for over 30,000 charge/discharge cycles, while the EMCCD was used to capture the light emission continuously for the first 10 cycles and at representative times for the remaining cycles.

Acknowledgements Part of this work was performed at the Stanford Nano Shared Facilities (SNSF), supported by the National Science Foundation under award ECCS-2026822.

Authors' contributions X.W., F.Y., Z.O. and G.H. conceived and designed the project; X.W., F.Y. and Z.O. performed the experiments; X.W., F.Y. and Z.O. analyzed the data and wrote the manuscript. All authors discussed the results and commented on the manuscript.

Funding G.H. acknowledges the support by a Rita Allen Foundation Scholars Award, a Beckman Technology Development Grant, a grant from the Spinal Muscular Atrophy (SMA) Foundation, a grant from the Focused Ultrasound (FUS) Foundation, a gift from the Pinetops Foundation, and seed grants from the Wu Tsai Neurosciences Institute and the Bio-X Initiative of Stanford University. X.W. acknowledges the support by a Stanford Graduate Fellowship. Z.O. acknowledges the support by a Wu Tsai Neurosciences Institute Interdisciplinary Scholar Award.

Data availability The authors declare that the data supporting the findings of this study are available within the paper. Should any raw data files be needed in another format they are available from the corresponding author upon reasonable request.

Declarations

Competing interests There are no competing interests to declare.

Open Access This article is licensed under a Creative Commons Attribution 4.0 International License, which permits use, sharing, adaptation, distribution and reproduction in any medium or format, as long as you give appropriate credit to the original author(s) and the source, provide a link to the Creative Commons licence, and indicate if changes were made. The images or other third party material in this article are included in the article's Creative Commons licence, unless indicated otherwise in a credit line to the material. If material is not included in the article's Creative Commons licence and your intended use is not permitted by statutory regulation or exceeds the permitted use, you will need to obtain permission directly from the copyright holder. To view a copy of this licence, visit <http://creativecommons.org/licenses/by/4.0/>.

References

1. Yao Y, Lei J, Shi Y, Ai F, Lu Y-C. Assessment methods and performance metrics for redox flow batteries. *Nat Energy*. 2021;6(6):582–8.
2. Sánchez-Díez E, Ventosa E, Guarnieri M, Trovò A, Flox C, Marcilla R, Soavi F, Mazur P, Aranzabe E, Ferret R. Redox flow batteries: status and perspective towards sustainable stationary energy storage. *J Power Sources*. 2021;481: 228804.
3. Li W, Zheng J, Hu B, Fu H-C, Hu M, Veyssal A, Zhao Y, He J-H, Liu TL, Ho-Baillie A, Jin S. High-performance solar flow battery powered by a perovskite/silicon tandem solar cell. *Nat Mater*. 2020;19(12):1326–31.
4. Li X, Lovell JF, Yoon J, Chen X. Clinical development and potential of photothermal and photodynamic therapies for cancer. *Nat Rev Clin Oncol*. 2020;17(11):657–74.
5. Cummins G, Cox BF, Ciuti G, Anbarasan T, Desmulliez MPY, Cochran S, Steele R, Plevris JN, Koulaouzidis A. Gastrointestinal diagnosis using non-white light imaging capsule endoscopy. *Nat Rev Gastroenterol Hepatol*. 2019;16(7):429–47.

6. Yang Y, Wu M, Vázquez-Guardado A, Wegener AJ, Grajales-Reyes JG, Deng Y, Wang T, Avila R, Moreno JA, Minkowicz S, Dumrongprechachan V, Lee J, Zhang S, Legaria AA, Ma Y, Mehta S, Franklin D, Hartman L, Bai W, Han M, Zhao H, Lu W, Yu Y, Sheng X, Banks A, Yu X, Donaldson ZR, Gereau RW, 4th, Good CH, Xie Z, Huang Y, Kozorovitskiy Y, Rogers JA. Wireless multilateral devices for optogenetic studies of individual and social behaviors. *Nat Neurosci.* 2021;24(7):1035–45.
7. Nihongaki Y, Kawano F, Nakajima T, Sato M. Photoactivatable CRISPR-Cas9 for Optogenetic Genome Editing. *Nat Biotechnol.* 2015;33(7):755–60.
8. Zhang J-C, Wang X, Marriott G, Xu C-N. Trap-controlled mechanoluminescent materials. *Prog Mater Sci.* 2019;103:678–742.
9. Yang F, Wu X, Cui H, Ou Z, Jiang S, Cai S, Zhou Q, Wong BG, Huang H, Hong G. A biomineral-inspired approach of synthesizing colloidal persistent phosphors as a multicolor, intravital light source. *Sci Adv.* 2022;8(30): eabo6743.
10. Yang F, Wu X, Cui H, Jiang S, Ou Z, Cai S, Hong G. Palette of rechargeable mechanoluminescent fluids produced by a biomineral-inspired suppressed dissolution approach. *J Am Chem Soc.* 2022;144(40):18406–18.
11. Jiang S, Wu X, Yang F, Rommelfanger NJ, Hong G. Activation of mechanoluminescent nanotransducers by focused ultrasound enables light delivery to deep-seated tissue in vivo. *Nat Protoc.* 2023;18(12):3787–820.
12. Feng A, Smet APF. A review of mechanoluminescence in inorganic solids: compounds, mechanisms, models and applications. *Materials.* 2018;11(4):484.
13. Van der Heggen D, Joos JJ, Rodríguez Burbano DC, Capobianco JA, Smet PF. Counting the photons: determining the absolute storage capacity of persistent phosphors. *Materials.* 2017;10(8):867.
14. Huang Y-P, Lin J-W. The trap bag concept of afterglow luminescence. *Sci Rep.* 2017;7(1):8475.
15. Wu X, Zhu X, Chong P, Liu J, Andre LN, Ong KS, Brinson K Jr, Mahdi AI, Li J, Fenno LE, Wang H, Hong G. Sono-optogenetics facilitated by a circulation-delivered rechargeable light source for minimally invasive optogenetics. *Proc Natl Acad Sci U S A.* 2019;116(52):26332–42.
16. Zhou XX, Fan LZ, Li P, Shen K, Lin MZ. Optical control of cell signaling by single-chain photoswitchable kinases. *Science.* 2017;355(6327):836–42.
17. Hong G. Seeing the sound. *Science.* 2020;369(6504):638.

Publisher's Note Springer Nature remains neutral with regard to jurisdictional claims in published maps and institutional affiliations.